

Resilient Full-Duplex ISAC in the Face of Imperfect SI Cancellation: Globally Optimal Timeslot Allocation and Beam Selection

Luis F. Abanto-Leon[†] and Setareh Maghsudi[§],

Ruhr University Bochum, Bochum, Germany

[†]Email: l.f.abanto@ieee.org [§]Email: setareh.maghsudi@ruhr-uni-bochum.de

Abstract—This work addresses the radio resource management (RRM) design in downlink full-duplex integrated sensing and communications (ISAC) systems, jointly optimizing timeslot allocation and beam selection under imperfect self-interference cancellation. Timeslot allocation governs the distribution of discrete channel uses between sensing and communication tasks, while beam selection determines transmit and receive directions along with adaptive beamwidths. The joint design leads to a semi-infinite, nonconvex mixed-integer nonlinear program (MINLP), which is difficult to solve. To overcome this, we develop a tailored reformulation strategy that transforms the problem into a tractable mixed-integer linear program (MILP), enabling globally optimal solutions. Our approach provides insights into the coordinated optimization of timeslot allocation and beam selection, enhancing the efficiency of full-duplex ISAC systems while ensuring resilience against residual self-interference.

Index Terms—Integrated sensing and communications, full-duplex, self-interference, beam selection, timeslot allocation.

I. INTRODUCTION

Integrated sensing and communications (ISAC) marks a groundbreaking advancement in wireless technology by seamlessly combining sensing and communications functionalities within the same hardware, spectrum, and waveform [1]. This tight integration promises to maximize radio resource utilization efficiency and reduce costs, enabling enhanced performance and capabilities across a wide range of applications.

Millimeter-wave and terahertz frequency bands are highly attractive for ISAC due to their short wavelengths, which enable high resolution for precise sensing [2], and their abundant spectrum availability, which supports high-throughput communications [3]. Prior works, e.g., [4], [5], have demonstrated the strong potential of combining ISAC with high-frequency bands to address the stringent connectivity and sensing requirements of future wireless systems.

At high frequencies, effective beamforming design is essential to unlock the full potential of ISAC. While digital beamforming offers high performance, its hardware complexity and costs scale unfavorably with frequency. This has driven growing interest in analog beamforming for ISAC, particularly in practical beam selection strategies, due to its cost-effectiveness and simple implementation [6]. However, most existing studies, with few exceptions (e.g., [7], [8]), considered beams with fixed beamwidth configurations. This assumption can be restrictive, as ISAC systems must accommodate diverse

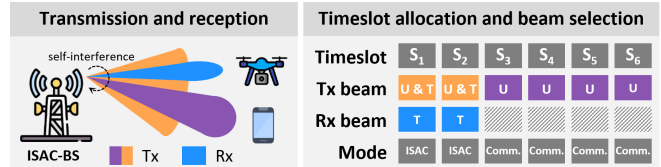


Fig. 1: System model comprising a BS, a user, and a target.

user and target requirements, necessitating adaptive beamwidth control. Furthermore, prior ISAC work predominantly focused on transmit-side beamforming, often overlooking the role of receive beamforming. *This motivates the need for an ISAC radio resource management (RRM) design that jointly optimizes beam direction and beamwidth at both the transmitter and receiver.*

Time allocation is another critical aspect in analog beamforming systems. With only a single radio-frequency (RF) chain, analog beamformers can process one signal at a time, requiring efficient time sharing to satisfy both sensing and communication demands. While time allocation has been extensively studied in the sensing literature, e.g., [9], and in the communication literature, e.g., [10], [11], only a limited number of studies have addressed this crucial aspect in the ISAC context, e.g., [12], [13]. Notably, [12] considered continuous-time allocation, whereas [13] focused on its discrete-time counterpart, the latter being particularly relevant, as it aligns with the timeslot-based structure of modern communication systems. *Therefore, a RRM design that incorporates timeslots as a key resource is crucial for meeting heterogeneous sensing and communication requirements, especially under the physical constraints of analog beamforming.*

To further improve resource utilization, full-duplex sensing has emerged as a promising paradigm [14]. However, its performance is fundamentally limited by self-interference (SI) [15]. While many existing studies assume either perfect SI cancellation or full knowledge of the SI channel, e.g., [16], [17], practical systems inevitably suffer from residual interference due to incomplete channel knowledge and hardware impairments. Such residual SI can critically degrade both communication and sensing performance. *Therefore, a RRM design that explicitly accounts for imperfect SI knowledge is essential to ensure resilient operation.*

Building on the above motivation, this paper investigates

a novel RRM problem for full-duplex ISAC systems that jointly optimizes timeslot allocation and beam selection, encompassing transmit/receive directions and beamwidths, while explicitly incorporating imperfect knowledge of residual SI. The resulting formulation yields a semi-infinite nonconvex mixed-integer nonlinear program (MINLP), which we systematically transform into an mixed-integer linear program (MILP) through a series of reformulations, enabling globally optimal solutions. Simulation results reveal insightful interdependencies in timeslot and beam sharing across functionalities, demonstrating how coordinated allocation can maximize overall resource efficiency.

Notation: Boldface capital letters \mathbf{X} and lowercase letters \mathbf{x} denote matrices and vectors, respectively. The transpose and Hermitian transpose of \mathbf{X} are denoted by \mathbf{X}^T and \mathbf{X}^H , respectively. Also, $\mathbb{E}\{\cdot\}$ denotes statistical expectation while $\mathcal{CN}(v, \xi^2)$ represents the complex Gaussian distribution with mean v and variance ξ^2 . Symbols $|\cdot|$ and $\|\cdot\|_2$ denote the absolute value and ℓ_2 -norm, respectively.

II. SYSTEM MODEL AND PROBLEM FORMULATION

A. Preliminaries

We consider an ISAC system in which a full-duplex base station (BS), equipped with N_{tx} transmit antennas and N_{rx} receive antennas, serves a single-antenna user and senses a single target. The BS operates in downlink mode and employs analog beamforming for transmission and reception. The transmit and receive beamformers can steer towards predefined angular directions, with multiple configurable beamwidths per direction. In addition, the BS employs timeslot allocation to efficiently meet the communication and sensing demands over a finite horizon of S timeslots. Each timeslot can be exclusively assigned to either communication or sensing, or configured to support both functionalities concurrently. In particular, the objective of the RRM design is to maximize communication throughput while ensuring that a specified number of sensing timeslots meet a predefined performance threshold. In the following, the s -th timeslot is denoted by \mathbf{S}_s , and the set of timeslots is defined as $\mathcal{S} = \{1, \dots, S\}$. The system model is depicted in Fig. 1, with a toy example described below.

Example: During timeslots \mathbf{S}_1 and \mathbf{S}_2 , the BS employs a broad beam (orange) to simultaneously serve the user (U) and illuminate the target (T) for sensing. This is feasible due to their proximate angular positions. With a higher angular misalignment, the target would be served alone, thereby needing timeslots for only sensing. A dedicated receive beam (blue) is simultaneously steered toward the target to collect echo signals. In \mathbf{S}_3 to \mathbf{S}_6 , the BS switches to a narrower, high-gain beam (purple) directed exclusively at the user, since the target's sensing requirements have already been fulfilled in the first two timeslots (according to predefined requirements). This allows the BS to concentrate the transmit power in the user's direction, thereby maximizing throughput.

B. Timeslot allocation

To determine which functionalities take place in each timeslot, we introduce constraints

$$\begin{aligned}\mathbf{C}_1 : \kappa_s &= \{0, 1\}, \forall s \in \mathcal{S}, \\ \mathbf{C}_2 : \zeta_s &= \{0, 1\}, \forall s \in \mathcal{S},\end{aligned}$$

where $\kappa_s = 1$ indicates that \mathbf{S}_s is used for communication, and $\kappa_s = 0$ otherwise. Similarly, $\zeta_s = 1$ indicates that \mathbf{S}_s is used for sensing, and $\zeta_s = 0$ otherwise.

To determine whether a given timeslot is active (i.e., used for communication, sensing, or both), we introduce constraint

$$\mathbf{C}_3 : \gamma_s = \kappa_s \vee \zeta_s, \forall s \in \mathcal{S}.$$

Here, $\gamma_s = 1$ indicates that \mathbf{S}_s is active, while $\gamma_s = 0$ indicates that \mathbf{S}_s is idle. Furthermore, we include constraint

$$\mathbf{C}_4 : \sum_{s \in \mathcal{S}} \gamma_s \leq S,$$

to ensure that the RRM design is confined within a finite horizon of S timeslots.

C. Beam selection

The BS can dynamically adjust the direction and beamwidth of its transmit and receive beampatterns, constrained to a finite set of possible configurations. We model this using a predefined codebook, where each codeword (i.e., codebook's element) corresponds to a unique combination of direction and beamwidth. Let D_{tx} denote the different angular directions in which the transmit signal can be steered. For each direction, we assume B_{tx} different beamwidths, leading to $L_{tx} = D_{tx}B_{tx}$ distinct transmit beampatterns. We denote the transmit codewords as $\mathbf{b}_b \in \mathbb{C}^{N_{tx} \times 1}$, such that $\|\mathbf{b}_b\|_2 = 1$, where $b \in \mathcal{L}_{tx}$ and $\mathcal{L}_{tx} = \{1, 2, \dots, L_{tx}\}$. A similar approach is adopted with the receive codewords, considering D_{rx} directions and B_{rx} beamwidths. This leads to $L_{rx} = D_{rx}B_{rx}$ distinct receive beampattern possibilities, with the receive codewords denoted by $\mathbf{c}_c \in \mathbb{C}^{N_{rx} \times 1}$, where $c \in \mathcal{L}_{rx}$ and $\mathcal{L}_{rx} = \{1, 2, \dots, L_{rx}\}$.

To enable transmit beamforming, we introduce constraint

$$\mathbf{C}_5 : \chi_{b,s} \in \{0, 1\}, \forall b \in \mathcal{L}_{tx}, s \in \mathcal{S},$$

where $\chi_{b,s} = 1$ indicates that codeword \mathbf{b}_b is used in \mathbf{S}_s , and $\chi_{b,s} = 0$ otherwise. Furthermore, we introduce constraint

$$\mathbf{C}_6 : \sum_{b \in \mathcal{L}_{tx}} \chi_{b,s} = \gamma_s, \forall s \in \mathcal{S},$$

to ensure that only one transmit codeword is selected for each active timeslot (see constraint \mathbf{C}_3). Thus, the transmit beamformer employed in \mathbf{S}_s is defined by constraint

$$\mathbf{C}_7 : \mathbf{t}_s = \sum_{b \in \mathcal{L}_{tx}} \mathbf{b}_b \cdot \chi_{b,s}, \forall s \in \mathcal{S}.$$

To enable receive beamforming, we introduce constraint

$$\mathbf{C}_8 : \rho_{c,s} \in \{0, 1\}, \forall c \in \mathcal{L}_{rx}, s \in \mathcal{S},$$

where $\rho_{c,s} = 1$ indicates that codeword \mathbf{c}_c is used in \mathbf{S}_s , and $\rho_{c,s} = 0$ otherwise. Additionally, we include constraint

$$\mathbf{C}_9 : \sum_{c \in \mathcal{L}_{rx}} \rho_{c,s} = \zeta_s, \forall s \in \mathcal{S},$$

to ensure that only one receive codeword is selected for each timeslot performing sensing (see constraint C_2). The receive beamformer used in S_s is given by constraint

$$C_{10} : \mathbf{r}_s = \sum_{c \in \mathcal{L}_{rx}} \mathbf{c}_c \cdot \rho_{c,s}, \forall s \in \mathcal{S}.$$

D. Communication metric

The signal transmitted by the BS in S_s is given by $\mathbf{x}_s = \mathbf{t}_s d_s$, where $d_s \in \mathbb{C}$ represents the symbol in S_s , which is used for either or both functionalities simultaneously. Symbol d_s follows a complex Gaussian distribution with zero mean and unit variance, e.g., $\mathbb{E}\{d_s d_s^*\} = 1$. The signal received by the user in S_s is

$$y_{\text{com}}^s = \mathbf{h}^H \mathbf{x}_s \cdot \kappa_s + n_{\text{com}} = \mathbf{h}^H \mathbf{t}_s d_s \cdot \kappa_s + n_{\text{com}}, \quad (1)$$

where $\mathbf{h} \in \mathbb{C}^{N_{tx} \times 1}$ is the communication channel between the BS and the user, while $n_{\text{com}} \sim \mathcal{CN}(0, \sigma_{\text{com}}^2)$ represents additive white Gaussian noise (AWGN). As a result, the communication signal-to-noise ratio (SNR) in S_s is given by

$$\text{SNR}_{\text{com}}^s = |\mathbf{h}^H \mathbf{t}_s \cdot \kappa_s|^2 / \sigma_{\text{com}}^2.$$

E. Sensing metric

We model the target as a far-field point source and consider a monostatic radar configuration at the BS, where the angle of departure (AOD) equals the angle of arrival (AOA), both denoted by θ . Additionally, the reflection coefficient (RC) captures both the target's radar cross-section and the round-trip path-loss relative to the BS, and is denoted by ψ . The sensing channel between the BS and the target is

$$\mathbf{G} = \psi \cdot \mathbf{a}_{\text{tx}}(\theta) \mathbf{a}_{\text{tx}}^H(\theta) = \psi \cdot \mathbf{A}(\theta), \quad (2)$$

where the transmit and receive steering vectors are given by $\mathbf{a}_l(\theta) = \frac{1}{\sqrt{N_l}} e^{j\phi_l \cos(\theta)}$, with $l = \{\text{tx, rx}\}$. Additionally, $\phi_l = \frac{2\pi d_l}{\lambda} \left[\frac{-N_l+1}{2}, \dots, \frac{N_l-1}{2} \right]^T$, λ is the wavelength, and d_l represents the spacing among antenna elements.

The signal reflected by the target and received by the BS during S_s is modeled as

$$\begin{aligned} y_{\text{sen}}^s &= \mathbf{r}_s^H (\mathbf{G} + \mathbf{Q}) \mathbf{x}_s \cdot \zeta_s + \mathbf{r}_s^H \mathbf{n}_{\text{sen}}, \\ &= \mathbf{r}_s^H \mathbf{G} \mathbf{t}_s d_s \cdot \zeta_s + \mathbf{r}_s^H \mathbf{Q} \mathbf{t}_s d_s \cdot \zeta_s + \mathbf{r}_s^H \mathbf{n}_{\text{sen}}, \end{aligned} \quad (3)$$

where \mathbf{Q} represents the direct SI channel between the transmit and receive arrays, while $\mathbf{n}_{\text{sen}} \sim \mathcal{CN}(\mathbf{0}, \sigma_{\text{sen}}^2 \mathbf{I})$ denotes AWGN at the BS's receiver. Specifically, \mathbf{Q} depends on the relative geometry between the arrays, and is modeled as

$$[\mathbf{Q}]_{\bar{m}, \bar{n}} = \frac{\lambda}{4\pi \bar{d}_{\bar{m}, \bar{n}}} \frac{1}{\sqrt{N_{tx} N_{rx}}} e^{-j \frac{2\pi}{\lambda} \bar{d}_{\bar{m}, \bar{n}}}, \quad (4)$$

where $\bar{d}_{\bar{m}, \bar{n}}$ represents the distance between the \bar{m} -th receive antenna and the \bar{n} -th transmit antenna [18], with the array centers spaced by distance \bar{d}_c .

To mitigate SI influence, the BS employs analog and/or digital signal processing techniques [19]. Leveraging an estimate of \mathbf{Q} , denoted by $\mathbf{Q}_{\text{est}} = (1 - v_{\text{si}}) \mathbf{Q}$, the BS subtracts $\mathbf{r}_s^H \mathbf{Q}_{\text{est}} \mathbf{t}_s d_s \cdot \zeta_s$ from y_{sen}^s , which results in

$$\begin{aligned} \bar{y}_{\text{sen}}^s &= y_{\text{sen}}^s - \mathbf{r}_s^H \mathbf{Q}_{\text{est}} \mathbf{t}_s d_s \cdot \zeta_s, \\ &= \mathbf{r}_s^H \mathbf{G} \mathbf{t}_s d_s \cdot \zeta_s + \mathbf{r}_s^H \mathbf{R} \mathbf{t}_s d_s \cdot \zeta_s + \mathbf{r}_s^H \mathbf{n}_{\text{sen}}. \end{aligned} \quad (5)$$

Here, $\mathbf{R} = \mathbf{Q} - \mathbf{Q}_{\text{est}} = v_{\text{si}} \mathbf{Q}$ is the residual SI channel, where v_{si} captures the imperfection in the SI cancellation process. A value of v_{si} close to 1 indicates poor cancellation performance (i.e., high residual interference), whereas a value near 0 reflects highly effective cancellation. Since v_{si} cannot be precisely known in practice, it is modeled as an uncertain parameter within a bounded interval

$$C_{11} : \Upsilon \triangleq \left\{ v_{\text{si}} \mid v_{\text{si}} = \bar{v}_{\text{si}} + \Delta v_{\text{si}}, |\Delta v_{\text{si}}|^2 \leq \epsilon^2 \right\},$$

imposing an infinite number of inequalities, where v_{si} is the actual but unknown SI factor, \bar{v}_{si} is the estimated SI factor, and Δv_{si} is random error whose power is bounded by ϵ^2 .

From (5), the target's sensing signal-to-interference-plus-noise ratio (SINR) during S_s is defined as

$$\text{SINR}_{\text{sen}}^s = |\mathbf{r}_s^H \mathbf{G} \mathbf{t}_s \cdot \zeta_s|^2 / \left(|\mathbf{r}_s^H \mathbf{R} \mathbf{t}_s \cdot \zeta_s|^2 + \sigma_{\text{sen}}^2 \|\mathbf{r}_s\|_2^2 \right).$$

Subsequently, we introduce constraint

$$C_{12} : \text{SINR}_{\text{sen}}^s \geq \Lambda_{\text{sinr}} \cdot \zeta_s, \forall s \in \mathcal{S},$$

which guarantees a predefined SINR threshold Λ_{sinr} for the target across its allocated timeslots. The minimum number of sensing timeslots is denoted by M_{sen} and is ensured through

$$C_{13} : \sum_{s \in \mathcal{S}} \zeta_s \geq M_{\text{sen}}.$$

F. Objective function

We define the objective function

$$f(\Omega) \triangleq \sum_{s \in \mathcal{S}} WT \log_2 (1 + \text{SNR}_{\text{com}}^s), \quad (6)$$

which represents the throughput. Here, T is the timeslot duration, W is the system's bandwidth, and Ω represents the set of all decision variables.

G. Problem formulation

We formulate the RRM design as

$$\mathcal{P}(\Omega) : \underset{\Omega}{\text{maximize}} \quad f(\Omega) \quad \text{s.t.} \quad \Omega \in \mathcal{X},$$

where \mathcal{X} is the feasible domain defined by $C_1 - C_{13}$. Problem $\mathcal{P}(\Omega)$ is a semi-infinite nonconvex MINLP that is challenging to solve due to variable couplings, its fractional structure, and an infinite number of constraints.

III. PROPOSED SOLUTION APPROACH

This section describes a sequence of transformation procedures applied to $\mathcal{P}(\Omega)$, resulting in an exact reformulation denoted by $\mathcal{P}'(\Omega')$. Specifically, Ω' represents the updated set of variables associated with the transformed problem.

Procedure 1. We substitute \mathbf{t}_s (as defined in C_7) into $f(\Omega)$, leading to

$$f_{\text{aux},1}(\Omega) \triangleq \sum_{s \in \mathcal{S}} WT \log_2 \left(1 + \left| \sum_{b \in \mathcal{L}_{tx}} \bar{\mathbf{h}}^H \mathbf{b}_b \cdot \chi_{b,s} \cdot \kappa_s \right|^2 \right),$$

where $\bar{\mathbf{h}} = \mathbf{h}/\sigma_{\text{com}}$. Considering any S_s , and applying Jensen's inequality to the absolute value term in $f_{\text{aux},1}$, yields

$$\mathbf{D}_{\text{aux},1} : \left| \sum_{b \in \mathcal{L}_{\text{tx}}} \bar{\mathbf{h}}^H \mathbf{b}_b \cdot \chi_{b,s} \cdot \kappa_s \right| \leq \sum_{b \in \mathcal{L}_{\text{tx}}} \left| \bar{\mathbf{h}}^H \mathbf{b}_b \cdot \chi_{b,s} \cdot \kappa_s \right|.$$

If \mathbf{b}_i denotes the transmit beamformer in S_s , then $\chi_{i,s} = 1$ and $\chi_{b,s} = 0, \forall b \in \mathcal{L}_{\text{tx}} \setminus \{i\}$. Hence, $\mathbf{D}_{\text{aux},1}$ simplifies to

$$\begin{aligned} \mathbf{D}_{\text{aux},2} : & \left| \sum_{b \neq i} \bar{\mathbf{h}}^H \mathbf{b}_b \cdot \chi_{b,s} \cdot \kappa_s + \bar{\mathbf{h}}^H \mathbf{b}_i \cdot \chi_{i,s} \cdot \kappa_s \right| \\ & \leq \sum_{b \neq i} \left| \bar{\mathbf{h}}^H \mathbf{b}_b \cdot \chi_{b,s} \cdot \kappa_s \right| + \left| \bar{\mathbf{h}}^H \mathbf{b}_i \cdot \chi_{i,s} \cdot \kappa_s \right|. \end{aligned}$$

Exponentiating both sides yields

$$\begin{aligned} \mathbf{D}_{\text{aux},3} : & \left| \sum_{b \neq i} \bar{\mathbf{h}}^H \mathbf{b}_b \cdot \chi_{b,s} \cdot \kappa_s + \bar{\mathbf{h}}^H \mathbf{b}_i \cdot \chi_{i,s} \cdot \kappa_s \right|^2 \leq \\ & \left(\sum_{b \neq i} \left| \bar{\mathbf{h}}^H \mathbf{b}_b \cdot \chi_{b,s} \cdot \kappa_s \right| \right)^2 + \left| \bar{\mathbf{h}}^H \mathbf{b}_i \cdot \chi_{i,s} \cdot \kappa_s \right|^2 + \\ & 2 \left(\sum_{b \neq i} \left| \bar{\mathbf{h}}^H \mathbf{b}_b \cdot \chi_{b,s} \cdot \kappa_s \right| \right) \left| \bar{\mathbf{h}}^H \mathbf{b}_i \cdot \chi_{i,s} \cdot \kappa_s \right|. \end{aligned}$$

The terms under the summations are zero, leading to $\left| \sum_{b \in \mathcal{L}_{\text{tx}}} \bar{\mathbf{h}}^H \mathbf{b}_b \cdot \chi_{b,s} \cdot \kappa_s \right|^2 = \sum_{b \in \mathcal{L}_{\text{tx}}} \left| \bar{\mathbf{h}}^H \mathbf{b}_b \cdot \chi_{b,s} \cdot \kappa_s \right|^2$ and allowing us to equivalently express $f_{\text{aux},1}(\Omega)$ as

$$f_{\text{aux},2}(\Omega) \triangleq \sum_{s \in \mathcal{S}} WT \log_2 \left(1 + \sum_{b \in \mathcal{L}_{\text{tx}}} \left| \bar{\mathbf{h}}^H \mathbf{b}_b \cdot \chi_{b,s} \cdot \kappa_s \right|^2 \right).$$

Leveraging the subadditivity property of the logarithm, we derive

$$\begin{aligned} \mathbf{D}_{\text{aux},4} : & \log_2 \left(1 + \sum_{b \in \mathcal{L}_{\text{tx}}} \left| \bar{\mathbf{h}}^H \mathbf{b}_b \cdot \chi_{b,s} \cdot \kappa_s \right|^2 \right) \leq \\ & \sum_{b \in \mathcal{L}_{\text{tx}}} \log_2 \left(1 + \left| \bar{\mathbf{h}}^H \mathbf{b}_b \cdot \chi_{b,s} \cdot \kappa_s \right|^2 \right). \end{aligned}$$

Recalling that $\chi_{i,s} = 1$ and $\chi_{b,s} = 0, \forall b \in \mathcal{L}_{\text{tx}} \setminus \{i\}$, we expand both sides of $\mathbf{D}_{\text{aux},4}$ and eliminate the zero-valued terms, as we did in $\mathbf{D}_{\text{aux},2}$. This reveals that the inequality in $\mathbf{D}_{\text{aux},4}$ is tight, allowing us to recast $f_{\text{aux},2}(\Omega)$ as

$$f'(\Omega') \triangleq \sum_{s \in \mathcal{S}} \sum_{b \in \mathcal{L}_{\text{tx}}} WT \log_2 \left(1 + \left| \bar{\mathbf{h}}^H \mathbf{b}_b \right|^2 \delta_{b,s} \right),$$

where $\delta_{b,s}$ are newly introduced variables, defined in

$$\mathbf{D}_{\text{aux},5} : \delta_{b,s} = \chi_{b,s} \kappa_s, \forall b \in \mathcal{L}_{\text{tx}}, s \in \mathcal{S}.$$

To cope with the coupling between variables $\chi_{b,s}$ and κ_s within $\mathbf{D}_{\text{aux},5}$, we use propositional calculus as in [20], [21], which decomposes $\mathbf{D}_{\text{aux},5}$ into

$$\begin{aligned} \mathbf{D}_1 : & \delta_{b,s} \leq \chi_{b,s}, \forall b \in \mathcal{L}_{\text{tx}}, s \in \mathcal{S}, \\ \mathbf{D}_2 : & \delta_{b,s} \leq \kappa_s, \forall b \in \mathcal{L}_{\text{tx}}, s \in \mathcal{S}, \\ \mathbf{D}_3 : & \delta_{b,s} \geq \chi_{b,s} + \kappa_s - 1, \forall b \in \mathcal{L}_{\text{tx}}, s \in \mathcal{S}, \\ \mathbf{D}_4 : & \delta_{b,s} \geq 0, \forall b \in \mathcal{L}_{\text{tx}}, s \in \mathcal{S}. \end{aligned}$$

As a result, $f(\Omega)$ is equivalently rewritten as $f'(\Omega')$, subject to including extra constraints \mathbf{D}_1 , \mathbf{D}_2 , \mathbf{D}_3 , and \mathbf{D}_4 .

Procedure 2. By rearranging the terms of \mathbf{C}_{12} , this constraint can be transformed into

$$\mathbf{E}_{\text{aux},1} : \left| \mathbf{r}_s^H \mathbf{G} \mathbf{t}_s \cdot \zeta_s \right|^2 \geq \zeta_s \Lambda_{\text{sinr}} \left| \mathbf{r}_s^H \mathbf{R} \mathbf{t}_s \right|^2 + \zeta_s \Lambda_{\text{sinr}} \sigma_{\text{sen}}^2 \left\| \mathbf{r}_s \right\|_2^2, \forall s \in \mathcal{S}.$$

Since ζ_s is binary and common to all terms in $\mathbf{E}_{\text{aux},1}$, it can be canceled from both sides¹, transforming $\mathbf{E}_{\text{aux},1}$ into

$$\mathbf{E}_{\text{aux},2} : \left| \mathbf{r}_s^H \mathbf{G} \mathbf{t}_s \right|^2 \geq \Lambda_{\text{sinr}} \left| \mathbf{r}_s^H \mathbf{R} \mathbf{t}_s \right|^2 + \Lambda_{\text{sinr}} \sigma_{\text{sen}}^2 \left\| \mathbf{r}_s \right\|_2^2, \forall s \in \mathcal{S}.$$

Leveraging \mathbf{C}_{11} and the definitions $\mathbf{G} = \psi \mathbf{A}(\theta)$ and $\mathbf{R} = v_{\text{si}} \mathbf{Q}$, we can reformulate $\mathbf{E}_{\text{aux},2}$ as

$$\mathbf{E}_{\text{aux},3} : \left| \mathbf{r}_s^H \mathbf{A}(\theta) \mathbf{t}_s \right|^2 \geq \max_{v_{\text{si}} \in \Upsilon} \frac{\Lambda_{\text{sinr}}}{|\psi|^2} v_{\text{si}}^2 \left| \mathbf{r}_s^H \mathbf{Q} \mathbf{t}_s \right|^2 + \frac{\Lambda_{\text{sinr}}}{|\psi|^2} \sigma_{\text{sen}}^2 \left\| \mathbf{r}_s \right\|_2^2, \forall s \in \mathcal{S}.$$

To improve tractability, we introduce a new set of variables, defined by

$$\mathbf{E}_1 : z_s \geq 0, \forall s \in \mathcal{S},$$

allowing us to split $\mathbf{E}_{\text{aux},3}$ into \mathbf{E}_2 and $\mathbf{E}_{\text{aux},4}$, shown below,

$$\mathbf{E}_2 : \left| \mathbf{r}_s^H \mathbf{A}(\theta) \mathbf{t}_s \right|^2 \geq z_s, \forall s \in \mathcal{S},$$

$$\begin{aligned} \mathbf{E}_{\text{aux},4} : z_s \geq & \max_{v_{\text{si}} \in \Upsilon} \frac{\Lambda_{\text{sinr}}}{|\psi|^2} v_{\text{si}}^2 \left| \mathbf{r}_s^H \mathbf{Q} \mathbf{t}_s \right|^2 + \\ & \frac{\Lambda_{\text{sinr}}}{|\psi|^2} \sigma_{\text{sen}}^2 \left\| \mathbf{r}_s \right\|_2^2, \forall s \in \mathcal{S}, \forall s \in \mathcal{S}. \end{aligned}$$

Note that $\mathbf{E}_{\text{aux},4}$ is equivalent to

$$\begin{aligned} \mathbf{E}_{\text{aux},5} : z_s \geq & \max_{|\Delta v_{\text{si}}|^2 \leq \epsilon^2} \frac{\Lambda_{\text{sinr}}}{|\psi|^2} (\bar{v}_{\text{si}} + \Delta v_{\text{si}})^2 \left| \mathbf{r}_s^H \mathbf{Q} \mathbf{t}_s \right|^2 + \\ & \frac{\Lambda_{\text{sinr}}}{|\psi|^2} \sigma_{\text{sen}}^2 \left\| \mathbf{r}_s \right\|_2^2, \forall s \in \mathcal{S}, \forall s \in \mathcal{S}, \end{aligned}$$

if we leverage \mathbf{C}_{11} . The maximum value of the right-hand-side (RHS) term in $\mathbf{E}_{\text{aux},5}$ is achieved when Δv_{si} has a positive sign and maximum magnitude, i.e., $\Delta v_{\text{si}} = \epsilon$. Hence, we can recast $\mathbf{E}_{\text{aux},5}$ as

$$\mathbf{E}_3 : z_s \geq \frac{\Lambda_{\text{sinr}}}{|\psi|^2} \left((\bar{v}_{\text{si}} + \epsilon)^2 \left| \mathbf{r}_s^H \mathbf{Q} \mathbf{t}_s \right|^2 + \sigma_{\text{sen}}^2 \left\| \mathbf{r}_s \right\|_2^2 \right), \forall s \in \mathcal{S},$$

As a result, constraints \mathbf{C}_{11} and \mathbf{C}_{12} can be recast equivalently as \mathbf{E}_1 , \mathbf{E}_2 , and \mathbf{E}_3 .

¹Note that canceling ζ_s from both sides of $\mathbf{E}_{\text{aux},1}$ is generally invalid if $\zeta_s = 0$. However, \mathbf{r}_s is a function of ζ_s , (through \mathbf{C}_9 and \mathbf{C}_{10}). Thus, if sensing is enabled, $\mathbf{r}_s \neq \mathbf{0}$ (as one codeword must be selected), which implies $\zeta_s = 1$ and justifies the cancellation. Conversely, if sensing is not enabled, then $\mathbf{r}_s = \mathbf{0}$ (through \mathbf{C}_9 and \mathbf{C}_{10}), reducing the inequality to $0 = 0$, which holds true as an equality. Hence, in this particular case where \mathbf{r}_s retains information about ζ_s , the variables ζ_s can be canceled on both sides.

Procedure 3. By applying propositional calculus as in [20], we eliminate the logical OR (\vee) in constraint C_3 , thereby transforming it into four equivalent constraints,

$$\begin{aligned}\text{F}_1 &: \gamma_s \leq \kappa_s + \zeta_s, \forall s \in \mathcal{S}, \\ \text{F}_2 &: \gamma_s \geq \kappa_s, \forall s \in \mathcal{S}, \\ \text{F}_3 &: \gamma_s \geq \zeta_s, \forall s \in \mathcal{S}, \\ \text{F}_4 &: \gamma_s \leq 1, \forall s \in \mathcal{S}.\end{aligned}$$

Consequently, C_3 is equivalent to F_1 , F_2 , F_3 , and F_4 .

Procedure 4. Substituting \mathbf{r}_s and \mathbf{t}_s (as defined in C_7 and C_{10}) into E_2 leads to

$$\text{G}_{\text{aux},1} : \left| \sum_{b \in \mathcal{L}_{\text{tx}}} \sum_{c \in \mathcal{L}_{\text{rx}}} \mathbf{c}_c^H \mathbf{A}(\theta) \mathbf{b}_b \rho_{c,s} \chi_{b,s} \right|^2 \geq z_s, \forall s \in \mathcal{S}.$$

Considering any \mathbf{S}_s and applying Jensen's inequality to the absolute value term in $\text{G}_{\text{aux},1}$, results in

$$\begin{aligned}\text{G}_{\text{aux},2} : \left| \sum_{b \in \mathcal{L}_{\text{tx}}} \sum_{c \in \mathcal{L}_{\text{rx}}} \mathbf{c}_c^H \mathbf{A}(\theta) \mathbf{b}_b \rho_{c,s} \chi_{b,s} \right| \leq \\ \sum_{b \in \mathcal{L}_{\text{tx}}} \sum_{c \in \mathcal{L}_{\text{rx}}} \left| \mathbf{c}_c^H \mathbf{A}(\theta) \mathbf{b}_b \rho_{c,s} \chi_{b,s} \right|.\end{aligned}$$

Assuming that \mathbf{b}_i and \mathbf{c}_j denote the transmit and receive beams used in \mathbf{S}_s leads to $\chi_{i,s} = 1$, $\rho_{j,s} = 1$, $\chi_{b,s} = 0$, $\forall b \in \mathcal{L}_{\text{tx}} \setminus \{i\}$, and $\rho_{c,s} = 0$, $\forall c \in \mathcal{L}_{\text{rx}} \setminus \{j\}$. As a result, $\text{G}_{\text{aux},2}$ collapses to

$$\begin{aligned}\text{G}_{\text{aux},3} : \left| \sum_{(b,c) \neq (i,j)} \mathbf{c}_c^H \mathbf{A}(\theta) \mathbf{b}_b \rho_{c,s} \chi_{b,s} + \mathbf{c}_j^H \mathbf{A}(\theta) \mathbf{b}_i \rho_{j,s} \chi_{i,s} \right| \\ \leq \sum_{(b,c) \neq (i,j)} \left| \mathbf{c}_c^H \mathbf{A}(\theta) \mathbf{b}_b \rho_{c,s} \chi_{b,s} \right| + \left| \mathbf{c}_j^H \mathbf{A}(\theta) \mathbf{b}_i \rho_{j,s} \chi_{i,s} \right|.\end{aligned}$$

Exponentiating both sides to the power of two and eliminating the zero-valued terms, as in **Procedure 1**, reveals that both sides of the inequality are identical. As a result, the absolute value and summation can be interchanged without affecting the result, allowing us to equivalently express $\text{G}_{\text{aux},1}$ as

$$\text{G}_{\text{aux},4} : \sum_{b \in \mathcal{L}_{\text{tx}}} \sum_{c \in \mathcal{L}_{\text{rx}}} \left| \mathbf{c}_c^H \mathbf{A}(\theta) \mathbf{b}_b \rho_{c,s} \chi_{b,s} \right|^2 \geq z_s, \forall s \in \mathcal{S}.$$

To eliminate the coupling among $\rho_{c,s}$ and $\chi_{b,s}$ in $\text{G}_{\text{aux},4}$, we introduce new variables, defined in

$$\text{G}_{\text{aux},5} : \pi_{b,c,s} = \rho_{c,s} \chi_{b,s}, \forall b \in \mathcal{L}_{\text{tx}}, c \in \mathcal{L}_{\text{rx}}, s \in \mathcal{S},$$

which enables us to transform $\text{G}_{\text{aux},4}$ into

$$\text{G}_1 : \sum_{b \in \mathcal{L}_{\text{tx}}} \sum_{c \in \mathcal{L}_{\text{rx}}} \left| \mathbf{c}_c^H \mathbf{A}(\theta) \mathbf{b}_b \pi_{b,c,s} \right|^2 \geq z_s, \forall s \in \mathcal{S}.$$

Leveraging propositional calculus, we decompose $\text{G}_{\text{aux},5}$ into

$$\begin{aligned}\text{G}_2 &: \pi_{b,c,s} \leq \chi_{b,s}, \forall b \in \mathcal{L}_{\text{tx}}, c \in \mathcal{L}_{\text{rx}}, s \in \mathcal{S}, \\ \text{G}_3 &: \pi_{b,c,s} \leq \rho_{c,s}, \forall b \in \mathcal{L}_{\text{tx}}, c \in \mathcal{L}_{\text{rx}}, s \in \mathcal{S}, \\ \text{G}_4 &: \pi_{b,c,s} \geq \chi_{b,s} + \rho_{c,s} - 1, \forall b \in \mathcal{L}_{\text{tx}}, c \in \mathcal{L}_{\text{rx}}, s \in \mathcal{S}, \\ \text{G}_5 &: \pi_{b,c,s} \geq 0, \forall b \in \mathcal{L}_{\text{tx}}, c \in \mathcal{L}_{\text{rx}}, s \in \mathcal{S}.\end{aligned}$$

as in [20]. Following a similar procedure as that used to convert $\text{G}_{\text{aux},1}$ into $\text{G}_{\text{aux},4}$, we can transform E_3 into

$$\begin{aligned}\text{G}_{\text{aux},6} : z_s \geq \frac{\Lambda_{\text{sinr}}}{|\psi|^2} (\bar{v}_{\text{si}} + \epsilon)^2 \sum_{b \in \mathcal{L}_{\text{tx}}} \sum_{c \in \mathcal{L}_{\text{rx}}} \left| \mathbf{c}_c^H \mathbf{Q} \mathbf{b}_b \pi_{b,c,s} \right|^2 + \\ \frac{\Lambda_{\text{sinr}}}{|\psi|^2} \sigma_{\text{sen}}^2 \left\| \mathbf{r}_s \right\|_2^2, \forall s \in \mathcal{S}, \forall s \in \mathcal{S},\end{aligned}$$

where the new variables $\pi_{b,c,s}$, introduced in $\text{G}_{\text{aux},5}$, have been adopted. Note that $\left\| \mathbf{r}_s \right\|_2^2$, which appears in $\text{G}_{\text{aux},6}$, can be transformed by leveraging C_{10} , leading to

$$\text{G}_{\text{aux},7} : \sum_{c' \in \mathcal{L}_{\text{rx}}} \sum_{c \in \mathcal{L}_{\text{rx}}} \mathbf{c}_{c'}^H \mathbf{c}_c \cdot \rho_{c',s} \cdot \rho_{c,s}.$$

Since only one receive beam is chosen per active timeslot, which we denote by \mathbf{c}_j , then the product $\rho_{c',s} \cdot \rho_{c,s}$ is zero unless $j = c = c'$. Thus, $\left\| \mathbf{r}_s \right\|_2^2 = \sum_{c \in \mathcal{L}_{\text{rx}}} \mathbf{c}_c^H \mathbf{c}_c \cdot \rho_{c,s} = \sum_{c \in \mathcal{L}_{\text{rx}}} \left\| \mathbf{c}_c \right\|_2^2 \cdot \rho_{c,s}$. Using this result, allows us to recast $\text{G}_{\text{aux},7}$ as

$$\begin{aligned}\text{G}_6 : z_s \geq \frac{\Lambda_{\text{sinr}}}{|\psi|^2} (\bar{v}_{\text{si}} + \epsilon)^2 \sum_{b \in \mathcal{L}_{\text{tx}}} \sum_{c \in \mathcal{L}_{\text{rx}}} \left| \mathbf{c}_c^H \mathbf{Q} \mathbf{b}_b \pi_{b,c,s} \right|^2 + \\ \frac{\Lambda_{\text{sinr}}}{|\psi|^2} \sigma_{\text{sen}}^2 \sum_{c \in \mathcal{L}_{\text{rx}}} \left\| \mathbf{c}_c \right\|_2^2 \cdot \rho_{c,s}, \forall s \in \mathcal{S}.\end{aligned}$$

Thus, C_7 , C_{10} , C_{12} , E_2 , and E_3 are equivalently transformed into G_1 , G_2 , G_3 , G_4 , G_5 , and G_6 .

The reformulated problem is expressed as

$$\mathcal{P}'(\Omega') : \underset{\Omega'}{\text{maximize}} \quad f'(\Omega') \quad \text{s.t.} \quad \Omega' \in \mathcal{X}',$$

where \mathcal{X}' is the feasible domain defined by C_1 , C_2 , $\text{C}_4 - \text{C}_6$, C_8 , C_9 , C_{13} , $\text{D}_1 - \text{D}_4$, E_1 , $\text{F}_1 - \text{F}_4$, and $\text{G}_1 - \text{G}_6$. Here, $\mathcal{P}'(\Omega')$ is a MILP which can be solved to global optimality.

REMARK 1. The worst-case computational complexity of solving $\mathcal{P}'(\Omega')$ is given by $\binom{S}{M_{\text{sen}}} L_{\text{rx}}^{M_{\text{sen}}} L_{\text{tx}}^{S-M_{\text{sen}}}$. However, due to the assumed channel invariance over the time horizon of S timeslots, we can impose that the first M_{sen} timeslots are allocated for sensing and the remaining timeslots for communication. This allows the complexity to be reduced to $L_{\text{rx}}^{M_{\text{sen}}} L_{\text{tx}}^{S-M_{\text{sen}}}$ without affecting optimality. However, in practice, the computational complexity is significantly lower because the problem is a MILP. These types of problems can be solved more efficiently using specialized off-the-shelf solvers that employ advanced techniques like branch-and-bound and cutting planes.

IV. SIMULATION RESULTS

We evaluate problem $\mathcal{P}'(\Omega')$ under various configurations using the Rician channel model. The communication channel is $\mathbf{h} = \gamma \mathbf{v}$, where γ accounts for large-scale fading and

$$\mathbf{v} = \sqrt{K/(K+1)} \mathbf{v}^{\text{LoS}} + \sqrt{1/(K+1)} \mathbf{v}^{\text{NLoS}}, \quad (7)$$

is the normalized small-scale fading, with $K = 100$ being the Rician fading factor. The line-of-sight (LoS) component is given by $\mathbf{v}^{\text{LoS}} = \frac{1}{\sqrt{N_{\text{tx}}}} e^{j\phi_{\text{tx}} \cos(\beta)}$, where β is the LoS angle,

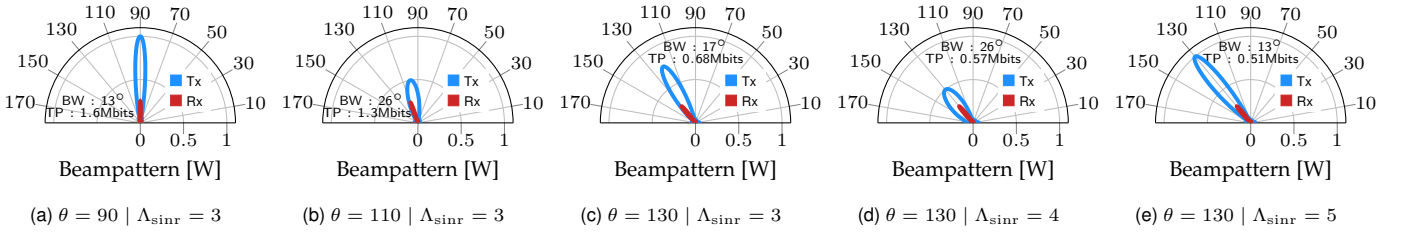


Fig. 2: Impact of user and target alignment on beam adaptation.

and the non-LoS (NLoS) components are defined as $\mathbf{v}^{\text{NLoS}} \sim \mathcal{CN}(\mathbf{0}, \mathbf{I})$. For large-scale fading, we adopt the UMa channel model [22], modeled as $\gamma = 28 + 22 \log_{10}(l) + 20 \log_{10}(f_c)$ dB, where $f_c = 41$ GHz is the carrier frequency, and $l = 60$ m is the distance between the BS and the user.

The communication and sensing noise powers are $\sigma_{\text{com}}^2 = -114$ dB and $\sigma_{\text{sen}}^2 = -74$ dB, respectively. The bandwidth is $W = 200$ MHz and the timeslot duration is $T = 1$ ms. The BS is equipped with uniform linear arrays (ULAs) consisting of $N_{\text{tx}} = 8$ transmit antennas and $N_{\text{rx}} = 16$ receive antennas. The transmit and receive directions span the interval from 50° to 130° with spacing of 5° degrees, yielding $D_{\text{tx}} = 17$ and $D_{\text{rx}} = 17$ distinct directions for transmission and reception, respectively². The beamwidths for transmission are $\{13^\circ, 17^\circ, 26^\circ, 60^\circ\}$, while the beamwidth options for reception are $\{6^\circ, 13^\circ, 17^\circ, 26^\circ\}$, leading to $B_{\text{tx}} = 4$ and $B_{\text{rx}} = 4$. The transmit and receive powers are set to 1 W and 0.25 W, respectively. The target's RC is $\psi = 6 \cdot 10^{-4}$ and the distance between array centers is $d_c = 0.15$ m. The results are averaged over 50 realizations unless specified otherwise.

A. Scenario I

We investigate how the transmit beam adapts to the relative angular positions of the user and target. To facilitate a clear visualization of this behavior, Fig. 2 considers a scenario with a single timeslot, thereby enforcing shared usage between sensing and communication (i.e., $S = S_{\text{sen}} = 1$). We assume the user remains fixed at $\beta = 90^\circ$, while the target moves across $\theta = \{90^\circ, 110^\circ, 130^\circ\}$. Throughout Fig. 2a to Fig. 2c, we set $\Lambda_{\text{sinr}} = 3$, while in Fig. 2d and Fig. 2e, we consider $\Lambda_{\text{sinr}} = 4$ and $\Lambda_{\text{sinr}} = 5$, respectively. Additionally, perfect SI cancellation is assumed ($\bar{v}_{\text{si}} = 0$ and $\epsilon = 0$).

In Fig. 2a, the user and target are perfectly aligned ($\theta = \beta = 90^\circ$), enabling the BS to employ the narrowest transmit beamwidth of 13° to service both. This results in a high throughput of 1.6 Mbits. In Fig. 2b, under moderate misalignment, the transmit beam steers towards 100° to approach the target direction (at $\theta = 110^\circ$) and widens its beamwidth to 26° to cover both user and target. As a result, the throughput decreases to 1.3 Mbits. In Fig. 2c, with greater misalignment ($\theta = 130^\circ$), the beam is steered further towards the target at 125° , to guarantee $\Lambda_{\text{sinr}} = 3$, but the throughput degrades

²In this work, the codewords are generated using the discrete Fourier transform. To broaden the beamwidth, the extreme elements of the arrays are switched off while the power is increased proportionally to maintain the same total transmit or receive power across codewords, as per the design condition specified in Section II-C.

significantly to 0.68 Mbits due to reduced energy radiated towards the user. In Fig. 2d, the sensing threshold increases to $\Lambda_{\text{sinr}} = 4$, prompting the beam to be centered at the target's AOD ($\theta = 130^\circ$) and to widen its beamwidth to 26° to ensure some energy also reaches the user, resulting in a reduced throughput of 0.57 Mbits. In Fig. 2e, with an even more stringent threshold of $\Lambda_{\text{sinr}} = 5$, the beam narrows back to 13° , concentrating primarily on the target. This tighter focus leads to a further drop in throughput to 0.51 Mbits, as only a minimal portion of the beam energy reaches the user. In all cases, the receive beam consistently points towards the target's AOD utilizing the narrowest available beamwidth of 6° to maximize sensing accuracy, as no SI is present.

B. Scenario II

We investigate how residual SI, the sensing SINR threshold, and the target's RC influence the throughput performance. The results are illustrated in Fig. 3, where we consider $\theta = 100^\circ$, $\Lambda_{\text{sinr}} \in \{1, 2, 3\}$, $S = 8$, $S_{\text{sen}} = 4$, $\bar{v}_{\text{si}} \in [0, 0.95]$, $\epsilon = 0.05$, and $\psi = \{6 \cdot 10^{-4}, 9 \cdot 10^{-4}\}$.

As \bar{v}_{si} increases, the throughput consistently decreases across all SINR thresholds. This degradation is attributed to elevated residual SI, which diminishes the effective sensing SINR. To compensate, the BS allocates more directive power towards the target, consequently reducing the energy radiated to the user. Additionally, increasing the sensing SINR threshold Λ_{sinr} also reduces throughput, particularly when \bar{v}_{si} is moderate to high. This is due to the need to steer more transmit power towards the target's AOD. Comparing the two RC scenarios, we observe that a larger RC (i.e., $\psi = 9 \cdot 10^{-4}$) has a favorable impact on throughput. Specifically, a higher RC enhances the sensing SINR without requiring the beam to be tightly aligned with the target's AOD. This allows more transmit power to be directed towards the user, thereby mitigating the throughput degradation caused by high SINR thresholds or elevated residual SI.

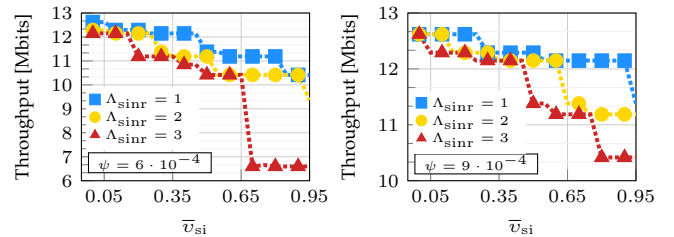


Fig. 3: Impact of residual SI and sensing threshold.

C. Scenario III

We investigate how the throughput is affected by the residual SI and the number of timeslots allocated for sensing. We adopt the same parameter settings as in *Scenario II*, with $\Lambda_{\text{sinr}} = 3$, $S_{\text{sen}} \in \{1, \dots, 8\}$, and $\psi = 6 \cdot 10^{-4}$. The throughput is visualized as a heatmap in Fig. 3.

For any fixed value of S_{sen} , the throughput consistently decreases as \bar{v}_{si} increases. This is because higher \bar{v}_{si} exacerbates the effect of residual SI on the sensing SINR, forcing the BS to employ increasingly directional beams steered towards the target's AOD to maintain sensing performance, a configuration that inherently reduces communication throughput. Additionally, for any fixed \bar{v}_{si} , throughput declines as S_{sen} increases, since more stringent sensing requirements constrain the resources available for throughput maximization. In contrast, neglecting residual SI significantly reduces reliability, yielding only 46.2% average feasibility over all cases, as shown in Fig. 4. This substantial performance gap underscores the necessity of explicitly incorporating residual SI into the RRM design to ensure robust operation.

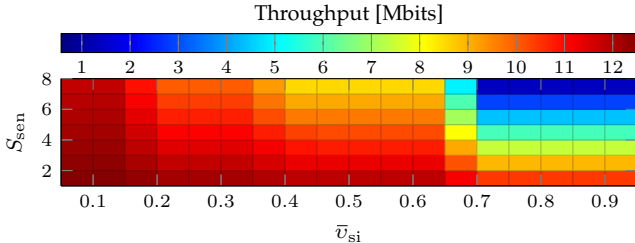


Fig. 4: Impact of residual SI and sensing timeslots.

D. Scenario IV

We investigate how the throughput is influenced by the separation between the transmit and receive arrays, which directly affects the severity of SI. We adopt the same parameter settings as in *Scenario III*, with $S_{\text{sen}} = 4$, and assume that no active SI cancellation is employed. Instead, SI is mitigated solely through physical array separation. The resulting throughput is depicted as a heatmap in Fig. 5.

The results show that increasing the separation distance \bar{d}_c has a beneficial impact on throughput. As \bar{d}_c grows, the influence of SI diminishes, allowing the BS to employ narrower, more directive beams towards the target's AOD without the risk of overwhelming SI power. Conversely, increasing the sensing SINR threshold Λ_{sinr} leads to a reduction in throughput, as more transmit power must be dedicated to meet the sensing requirement. The white regions indicate infeasible allocations where the SI is too severe to satisfy the sensing SINR threshold. We observe that a separation distance of 50 cm is sufficient to mitigate the impact of SI to acceptable levels. In particular, at this distance, the resulting throughput remains within 12% of the ideal case with hypothetically infinite separation, indicating that a distance of 50 cm offers a practical balance between SI cancellation and transceiver footprint.

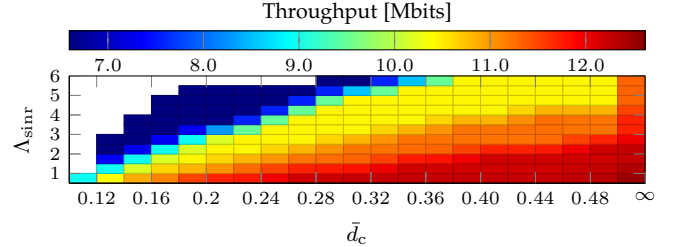


Fig. 5: Impact of array separation.

V. CONCLUSIONS

This paper investigated a novel RRM problem, jointly addressing timeslot allocation and beam adaptation under practical considerations, including discrete beam directions and beamwidths, and imperfect SI cancellation. To tackle the inherent complexity of the RRM problem, we proposed a tractable solution by reformulating the problem as a MILP, thereby ensuring reliable performance even under uncertainty in the residual SI level. Our results revealed how user-target angular alignment significantly influences system performance, with beam adaptation serving as a key mechanism to balance sensing and communication demands. Furthermore, we examined the effects of residual SI on throughput, and showed that increasing the physical separation between transmit and receive arrays offers a means of mitigating SI.

ACKNOWLEDGMENT

The authors acknowledge the financial support by the Federal Ministry for Research, Technology and Space (BMFTR) in Germany in the programme of “Souverän. Digital. Vernetzt.” Joint project 6G-RIC, project identification number: 16KISK035.

REFERENCES

- [1] A. R. Balef, S. Maghsudi, and S. Stanczak, “Adaptive energy-efficient waveform design for joint communication and sensing using multiobjective multiarmed bandits,” in *Proc. of WSA & SCC*, 2023, pp. 1–6.
- [2] G. Yao and Y. Pi, “Terahertz active imaging radar: preprocessing and experiment results,” *EURASIP J. Wirel. Commun. Netw.*, vol. 10, no. 1, pp. 1–8, 2014.
- [3] R. Askar, J. Chung, L. John, T. Merkle, S. Wittig, M. Schmieder, Y. Suh, J. Lee, B. Baumann, M. Peter, T. Haustein, W. Keusgen, and S. Stanczak, “Mobilizing the terahertz beam: D-band analog-beamforming front-end prototyping and long-range 6G trials,” *IEEE Wireless Commun.*, pp. 1–8, 2024.
- [4] Y. Zhuo, T. Mao, H. Li, C. Sun, Z. Wang, Z. Han, and S. Chen, “Multi-beam integrated sensing and communication: State-of-the-art, challenges and opportunities,” *IEEE Commun. Mag.*, vol. 62, no. 9, pp. 90–96, 2024.
- [5] L. F. Abanto-Leon and S. Maghsudi, “Hierarchical functionality prioritization in multicast ISAC: Optimal admission control and discrete-phase beamforming,” *IEEE Commun. Lett.*, pp. 1–5, 2024.
- [6] R. Zhao, T. Woodford, T. Wei, K. Qian, and X. Zhang, “M-Cube: A millimeter-wave massive MIMO software radio,” in *Proc. of ACM MobiCom*, 2020.
- [7] Z. Du, F. Liu, W. Yuan, C. Masouros, Z. Zhang, S. Xia, and G. Caire, “Integrated sensing and communications for V2I networks: Dynamic predictive beamforming for extended vehicle targets,” *IEEE Trans. Wireless Commun.*, vol. 22, no. 6, pp. 3612–3627, 2023.
- [8] H. Zhang, T. Yang, X. Wu, Z. Guo, and B. Hu, “Robust beamforming design for UAV communications based on integrated sensing and communication,” *J. Wireless Com. Network*, vol. 88, pp. 1–24, 2023.

- [9] H. Zhang, W. Liu, J. Yan, J. Shi, and Q. Zhang, "A fast solver for dwell time allocation in a phased array radar," *IEEE Trans. Veh. Technol.*, vol. 72, no. 8, pp. 10 345–10 356, 2023.
- [10] L. F. Abanto-Leon, M. Hollick, and G. H. Sim, "Hydrawave: Multi-group multicast hybrid precoding and low-latency scheduling for ubiquitous Industry 4.0 mmWave communications," in *Proc. of IEEE WoWMoM*, 2020, pp. 98–107.
- [11] V.-D. Nguyen, H. D. Tuan, T. Q. Duong, O.-S. Shin, and H. V. Poor, "Joint fractional time allocation and beamforming for downlink multiuser MISO systems," *IEEE Commun. Lett.*, vol. 21, no. 12, pp. 2650–2653, 2017.
- [12] D. Xu, Y. Xu, Z. Wei, S. Song, and D. W. Kwan Ng, "Sensing-enhanced secure communication: Joint time allocation and beamforming design," in *Proc. of WiOpt*, 2023, pp. 673–680.
- [13] L. Wang and L. F. Abanto-Leon, "Resource allocation for ISAC networks with application to target tracking," in *Proc. of IEEE GLOBECOM Workshops*, 2024, pp. 1–7.
- [14] B. Smida, A. Sabharwal, G. Fodor, G. C. Alexandropoulos, H. A. Suraweera, and C.-B. Chae, "Full-duplex wireless for 6G: Progress brings new opportunities and challenges," *IEEE J. Sel. Areas Commun.*, vol. 41, no. 9, pp. 2729–2750, 2023.
- [15] R. Hernangómez, J. Fink, R. L. Cavalcante, Z. Utkovski, and S. Stańczak, "Optimized detection with analog beamforming for monostatic integrated sensing and communication," in *Proc. of IEEE ICC*, 2024, pp. 317–323.
- [16] T. Xu, Z. He, J. Xu, W. Xu, J. Wang, and D. W. K. Ng, "Robust ISAC transceiver beamforming design under low-resolution AD/DA converters," *IEEE Wireless Commun. Lett.*, pp. 1–6, 2025.
- [17] T. Jiang, M. Jin, Q. Guo, Y. Liu, Y. Li, and J. Yao, "Full-duplex ISAC-enabled D2D underlaid cellular networks: Joint transceiver beamforming and power allocation," *IEEE Trans. on Cogn. Commun. Netw.*, pp. 1–13, 2025.
- [18] Z. Wang, X. Mu, and Y. Liu, "Near-field integrated sensing and communications," *IEEE Commun. Lett.*, vol. 27, no. 8, pp. 2048–2052, 2023.
- [19] S.-M. Kim, Y.-G. Lim, L. Dai, and C.-B. Chae, "Performance analysis of self-interference cancellation in full-duplex massive MIMO systems: Subtraction versus spatial suppression," *IEEE Trans. Wireless Commun.*, vol. 22, no. 1, pp. 642–657, 2023.
- [20] L. F. Abanto-Leon, A. Krishnamoorthy, A. Garcia-Saavedra, G. H. Sim, R. Schober, and M. Hollick, "Radio resource management design for RSMA: Optimization of beamforming, user admission, and discrete/continuous rates with imperfect SIC," *IEEE Trans. Mobile Comput.*, vol. 23, no. 12, pp. 11 498–11 518, 2024.
- [21] L. F. Abanto-Leon and S. Maghsudi, "Optimal user and target scheduling, user-target pairing, and low-resolution phase-only beamforming for ISAC systems," *IEEE Trans. Veh. Technol.*, pp. 1–6, 2025.
- [22] 3GPP, "Study on channel model for frequencies from 0.5 to 100 GHz," 3rd Generation Partnership Project (3GPP), Technical Report (TR) 38.901, 2020, version 16.1.0.